Nuclear Engineering and Technology 54 (2022) 4244–4252

Contents lists available at ScienceDirect

Nuclear Engineering and Technology

journal homepage: www.elsevier.com/locate/net

Original Article

Development and verification of a novel system for computed tomography scanner model construction in Monte Carlo simulations

Ying Liu [a], Ting Meng [a], Haowei Zhang [a, **], Qi Su [b], Hao Yan [b], Heqing Lu [b, *]

[a] School of Health Science and Engineering, University of Shanghai for Science and Technology, Shanghai, 200093, China
[b] Department of Medical Equipment, Shanghai First Maternity and Infant Hospital, School of Medicine, Tongji University, Shanghai, 200092, China

ARTICLE INFO

Article history:
Received 21 July 2021
Received in revised form
22 May 2022
Accepted 4 July 2022
Available online 13 July 2022

Keywords:
Monte Carlo simulations
CT scanner model
Energy spectrum
BT filter

ABSTRACT

The accuracy of Monte Carlo (MC) simulations in estimating the computed tomography radiation dose is highly dependent on the accuracy of CT scanner model. A system was developed to observe the 3D model intuitively and to calculate the X-ray energy spectrum and the bowtie (BT) filter model more accurately in Monte Carlo N-particle (MCNP). Labview's built-in Open Graphics Library (OpenGL) was used to display basic surfaces, and constructive solid geometry (CSG) method was used to realize Boolean operations. The energy spectrum was calculated by simulating the process of electronic shooting and the BT filter model was accurately modeled based on the calculated shape curve. Physical data from a study was used as an example to illustrate the accuracy of the constructed model. RMSE between the simulation and the measurement results were 0.97% and 0.74% for two filters of different shapes. It can be seen from the comparison results that to obtain an accurate CT scanner model, physical measurements should be taken as the standard. The energy spectrum library should be established based on Monte Carlo simulations with modifiable input files. It is necessary to use the three-segment splicing modeling method to construct the bowtie filter model.

1. Introduction

Computed tomography (CT) is a common medical imaging technique, and the radiation dose of patients has aroused great attention. Monte Carlo (MC) simulations are a popular method to accurately calculate radiation dose. However, researchers encounter two main problems when describing the CT scanner model in Monte Carlo N-particle (MCNP), one of the most widely used pieces of MC simulation software [1]. The first one is how to write an input file (including the source card, cell card, and tally card) to construct a CT scanner model. The structure of the input file is complex, and the drawing function of MCNP is limited to two-dimensional (2D) structures. This makes descriptions of complex geometries quite prone to errors [2]. The second problem is how to obtain an accurate CT scanner model to ensure the accuracy of the dose calculation. A CT scanner model requires a detailed description of the X-ray energy spectrum, bowtie (BT) filter thickness, and the geometry of the scanner.

Many studies have proposed methods for constructing CT scanner models in Monte Carlo simulations. Jarry et al. first proposed a LightSpeed 16 CT scanner system which was constructed based on the energy spectrum and filter parameters given by the manufacturer [3]. However, Turner et al. has proved that simulations using the equivalent source models based on physical measurements attained more accuracy than simulations using source models based on manufacturer's data [4]. Gu et al. also constructed a LightSpeed 16 CT scanner system, but they used an energy spectrum software to obtain the energy spectrum and simplified geometric model to describe the bowtie, which would cause larger errors [5]. Lee et al. used weighting factors based on a lateral free-in-air dose profile to replace explicit model of the external bowtie filter, which ignored the bowtie material and X-ray scattering [6]. It has been verified the equivalent spectrum obtained by matching the measured half-value layer (HVL) and the bowtie model constructed by calculating the BT profile (air kerma values as a function of fan angle) have obtained better accuracy in the MC simulations [7–12]. However, at present, different energy spectrum software developed a long time ago were still used in their studies. The

* Corresponding author. No.2699, West Gaoke Road, Pudong New District, Shanghai, China.
** Corresponding author. No.580, Jungong Road, Yangpu District, Shanghai, China.
E-mail addresses: howiezh@aliyun.com (H. Zhang), luheqing0811@126.com (H. Lu).

https://doi.org/10.1016/j.net.2022.07.004

database of these software cannot meet the characteristics of some new types of X-ray tubes because they have limitations on tube voltage and target material [13–16], which may also affect the accuracy of the scanner model. Therefore, in order to ensure the accuracy of the constructed CT scanner model in MC simulations, it is necessary to obtain the energy spectrum according to the actual situation of the tube, and to obtain the bowtie filter model based on physical measurements.

In this study, a novel system named Computed Tomography Model Designer (CTMD) was developed to help researchers obtain an accurate CT scanner model by the energy spectrum calculation part with adjustable internal parameters and BT filter calculation part based on provided physical measurements, and to increase the user-friendliness of MCNP by three-dimensional (3D) display and automatically generating input files.

In this paper, the 3D display method used in this system was first briefly described. Then, the calculation process and model construction method of the X-ray energy spectrum and bowtie filter based on provided physical measurements will be illustrated in detail. The accuracy of the CT scanner model constructed by this system will be assessed by comparing the simulation results and measurement results from other study. Finally, methods to improve the accuracy of the CT scanner model were discussed after analyzing the comparison results.

2. Materials and methods

2.1. Development environment

The writing style of input files generated by the system in this study were derived from MCNP5. In fact, the input files of the different versions of the MCNP program are written in approximately the same way [17]. LabVIEW (version 19.0) was used as the main development system, and the development platform was 64-bit Windows 10. The CPU was Ryzen 7 5800X, and the clock speed and running memory of the computer were 3.8 GHz and 8 GB, respectively. LabVIEW uses the graphical programming language G to write programs, and the resulting programs are in the form of block diagrams. LabVIEW's powerful features are attributed to its hierarchical structure, which makes it more convenient for subsequent modification and debugging of the software and secondary development [18].

2.2. MCNP code and 3D model display

2.2.1. Surface construction

MCNP constructs a 3D geometry by performing Boolean operations on several specified surfaces. These surfaces are generated by LabVIEW's 3D picture controls. Several special macros such as elliptical cylindrical surfaces were generated by stretching and deforming a cylindrical surface. Planes were generated by rotating and translating a box surface that lied in the x-y plane and whose thickness tended to be zero. Rodriguez rotation formula was used to rotate any plane in space as shown in equation (1).

$$v' = \cos\theta v + (1 - \cos\theta)(u \cdot v)u + \sin\theta u \times v \quad (1)$$

Here, θ is the rotation angle, u is the unit vectors of the rotation axis, v is the legal vector of the plane before rotation, and v' is the legal vector after rotation.

Using this method, CTMD can automatically calculate general equation coefficients for any plane moved by users. Each user-built surface can be deleted, translated, rotated, and zoomed in and out; all user-defined surfaces are recorded in the summary table on the right side. When a surface is clicked, the corresponding surface in the 3D view window will turn red, which makes it easy for users to quickly find the target surface.

2.2.2. Boolean operation

Complex geometries are constructed by Boolean operations between two or more surfaces. According to the manual of MCNP, to perform Boolean operations, users need to judge the direction of each surface and connect them with designated symbols (: for merge, space for intersection, and # for remainder). These steps can increase the possibility of geometric errors [1]. In this study, constructive solid geometry (CSG) method was used to complete Boolean operations because the advantages of CSG method are that it was concise, generated fast, and recorded in detail the original feature parameters.

The principle of performing Boolean operations in LabVIEW is shown in Fig. 1. Each regular surface consists of a set of points that satisfy the equation, and the process of Boolean operation is essentially a process of filtering the set of points. Starting with two surfaces, the points that satisfy the equation of surface A (Q (n) < 0) and surface B (P (m) < 0) were substituted into each other. This led to four cases each corresponding to a sequence of letters (xx, yy, xy, yx) that represent different Boolean operation symbols. By reading the sequence of letters, the set of points after each operation were filtered out. When a new surface was added, another judgment as above would update the letter sequence. The above judgment process was continuously looped until the final Boolean operation so that the target 3D geometry was finally rounded up.

2.3. CT scanner model calculation

2.3.1. Calculation of the X-ray energy spectrum

In the vacuum glass cover of the X-ray tube, electrons fly from the cathode to the anode target surface at high speed. Part or all of its kinetic energy becomes the energy of the generated photon resulting in Bremsstrahlung radiation. When the tube voltage of the X-ray tube exceeds a certain critical voltage (the excitation voltage of the target element), there will be characteristic radiation [19]. For energy spectrum calculations, the accuracy of Birch and Marshall's semi-empirical model algorithm was insufficient [14], and the energy spectrum obtained by Rogers et al. used MC simulation (BEAMnrc) to more accurately describe the particle transportation process [15]. Poludniowski et al. developed an energy spectrum program (SpekCalc) that combines elements of the above two methods; the accuracy of MC simulation was confirmed in their study [16]. Therefore, the simulation results of electron bombardment under different conditions can be used as a database of the X-ray energy spectrum analysis module.

The specific simulation method was as follows: In MCNP5, a vertically emitting electron source was set 6 cm away from the target surface, and the angle formed by the target surface and the Y axis was the anode angle. The thickness of the target surface was about 5 mm. A certain thickness of filtration was set 15 cm from the focal point, i.e., the inherent filtration of the X-ray tube [20]. The lower surface of the filtration was used to record the photon fluence in each energy bin. Data libraries used for electron-photon transport were mcplib04 and el03, which can be found in the Appendix G of the manual [21]. It was necessary to ensure that the error of the calculation result of each energy bin was within 10%, and the error of the total calculation result was within 1% so that the calculation result of the energy spectrum was reliable. Simulations were performed for 10^8 histories, and the width of energy bins was set to 1 keV. In the case of a single thread, it takes about 600 min to simulate each situation with the computer described in Section 2.1.

Several important parameters were then calculated. According to the X-ray energy spectrum obtained, the air kerma K^{Air} can be calculated using equation (2) [22]:

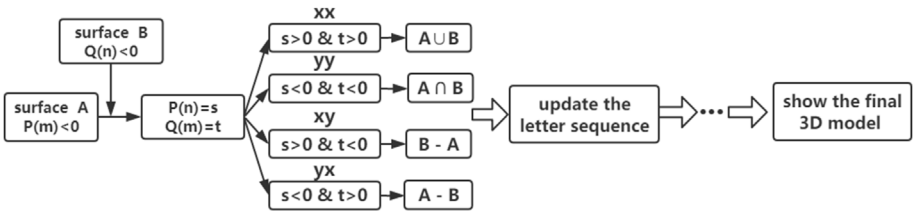

Fig. 1. The principle of performing Boolean operations in LabVIEW.

$$K^{Air} = \sum_{i=1}^{n} \Phi i Ei \left(\frac{\mu tr}{\rho}\right)_i^{Air} \tag{2}$$

where n is the total number of energy boxes, and Φ_i, E_i, and (μ_{tr}/ρ) are the photon fluence, average energy, and mass energy transfer coefficient of air of the i_{th} energy bin, respectively.

The mass-energy-transfer coefficients of air are equal to the mass-energy-absorption coefficients (μ_{en}/ρ) for photon energies less than 1 MeV [23], and the mass-energy-absorption coefficients can be found in the NIST report. The half-value layer (HVL) of X-rays is the thickness of the specified material that reduces the air kerma of the radiation beam to half of its initial value, which is usually expressed in terms of the thickness of the aluminum sheet (mm). Based on the X-ray energy spectrum, HVL can be obtained using equation (3) [22]:

$$\frac{1}{2}\sum_{i=1}^{n} K_i^{Air} = \sum_{i=1}^{n} K_i^{Air} \exp\left[-(\mu i)^{Al} HVL\right] \tag{3}$$

where K^{Air} and μ_i^{Al} are respectively the air kerma and attenuation coefficient of aluminum for the i_{th} energy bin. The photon energy corresponding to the linear attenuation coefficient of Al calculated by equation (4) [22] is the effective energy (E_{eff}) of the X-ray energy spectrum:

$$\left(\frac{\mu}{\rho}\right)^{Al} = \frac{\ln 2}{HVL} \tag{4}$$

The average energy of X-rays (E_{mean}) can be calculated using equation (5) [22].

$$Emean = \sum_{i=1}^{n} fiEi \tag{5}$$

where f_i is the percentage of the number of photons in each energy bin.

2.3.2. Calculation of the bowtie filter thickness

Several important geometric parameters and physical measurements of HVL and BT filter profiles are required to calculate the BT filter thickness. Geometric parameters can be easily obtained from the manufacturer including the distance from the focal spot to the isocenter (SID), the distance from the focal spot to the detector (SDD), the distance from the focal spot to the bowtie (SFD), and the fan angle [8–10].

For HVL measurements, many studies have described the measurement process [5,7,12], and thus this study will not go into detail. Several methods have been proposed for the BT filter profile measurements. Of these, the static X-ray source measurement is the simplest because there are no restrictions on measuring instruments and conditions [11,12]. Fig. 2 Shows a schematic view of the BT profile measurements across the fan angle of the static X-ray source. The X-ray tube is fixed at a direction of 90°. The distance from the i_{th} measuring point to the isocenter is L_i; thus, the beam angle can be calculated using equation (6):

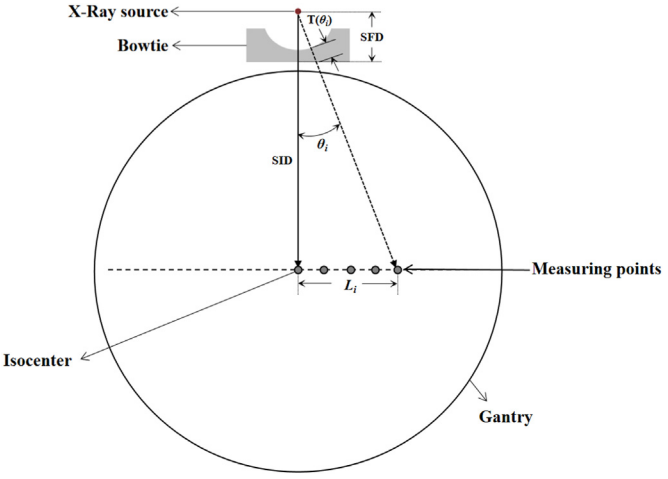

Fig. 2. BT profile measurements of the static X-ray source. L is the distance from the measurement point to the isocenter, θ is the beam angle, SID is the distance from the focal point to the isocenter, SFD is the distance from the focal point to the bowtie, and $T(\theta)$ is the bowtie filter thickness at the beam angle of θ. The grey dots represent different measurement points.

$$\theta i = \arctan\left(\frac{Li}{SID}\right) \tag{6}$$

The ionization chamber was initially centered at the scanner isocenter. Using fixed scan parameters, a 100-mm-length ionization chamber was used to measure the air kerma at multiple equally spaced measuring points. Finally, the BT filter profile as a function of the fan angle is obtained.

After all of the above parameters are obtained, the BT filter thickness can be calculated in four steps: (1) The ratios of the air kerma at all measuring points to that at isocenter are calculated based on the data to obtain a normalized air kerma curve as a function of fan angle. (2) The equivalent spectrum at the same tube voltage is obtained by matching measured and calculated HVL values. (3) When the equivalent spectrum passes through a certain thickness of filter, the subsequent air kerma can be calculated. A new ratio is thus obtained. Gradual increases in filter thickness were used until the calculated new ratio is equal to the measured ratio in step (1). (4) According to the SFD provided by the user, the BT thickness as a function of fan angle will be converted into a curve located in the Cartesian coordinate system. The BT filter shape can be obtained by fitting the thickness curve.

2.4. CT scanner model construction in MC simulation

For the X-ray source, the equivalent energy spectrum obtained is used to describe the sampling probability of the photon in each energy bin, the sampling angle can be used to describe the divergence angle of the photon, and the cookie cutter method is used to

Table 1
Adjustable parameters of the CT model used for generation of MCNP's input files.

Geometric parameters	Scanning parameters	Data files of physical measurements
SID	collimation	BT filter profile
SDD	FOV	Bowtie filter material
SFD	Pitch*	HVL
Beam angle	Tube voltage	Voxel matrix of the phantom
Beam geometry	Tube current	

SID = distance from the focal spot to the isocenter; SDD = distance from the focal spot to the detector; SFD = distance from the focal spot to the bowtie filter; FOV = field of view; HVL = half-value layer.

limit the radiation area. The bowtie filter shape is generated after the physical quantity is calculated, and based on this shape, Boolean operations are used to construct an equivalent 3D bowtie model. For the scanning model, a constantly moving source cannot be simulated in MCNP; thus, the result of several calculation files is usually superimposed to describe the rotation process of the X-ray tube. According to verified studies, 16 sources can be arranged in a week to simulate one rotation [24,25]. Table 1 shows the CT parameters that can be adjusted by the user in the system including geometric parameters and scanning parameters.

2.5. Verification simulation

In order to verify the accuracy of the CT scanner model, the static X-ray tube experiment needs to be simulated. The model of the ionization chamber and the scanning parameters of the experiment need to be accurately simulated, and the measured air kerma can be regarded as the deposition energy received by the effective air volume in the ionization chamber. Except for the bowtie filter and the ionization chamber, the rest is air. The number of photons is set to at least 10^8, so that the error of the simulation result is within 1%. In the case of a single thread, it takes about 3 min to simulate each situation with the computer described in Section 2.1.

3. Results

3.1. Comparison of parameters between this system and other X-ray energy spectrum software

Several important parameters (HVL, E_{mean} and E_{eff}) were compared with other energy spectrum software to verify the accuracy of the simulation results of X-ray energy spectrum based on MCNP5 in this study. For comparison, all spectra were assigned to 2 keV bin widths and normalized to unit area. When the tube voltages were 50 keV and 70 keV, the anode angle was set to 10° and the thickness of the aluminum sheet is 2.5 mm. When the tube voltages were 100 keV and 140 keV, the anode angle was set to 16°, and the thickness of the aluminum sheet was 5 mm [7].

The calculation results are shown in Table 2 along with those of BEAMnrc, SpekCalc, and IPEM78 [16]. The result of E_{mean} and E_{eff} of this system agreed well with those in other energy spectrum software. For HVL, the maximum discrepancy between CTMD and IPEM78 was 3%, the maximum discrepancy between CTMD and BEAmnrc was 5%, and the maximum discrepancy between CTMD and SpekCalc was 8%. The HVL value of CTMD at low tube voltage was closer to IPEM78 while the HVL value of CTMD at high tube voltage was closer to BEAMnrc. For E_{mean} and E_{eff}, the maximum discrepancies between CTMD and other three software were less than 3%. In all cases, the E_{mean} and E_{eff} predictions of CTMD were closer to those of IPEM78 than those of BEAMnrc and SpekCalc. Fig. 3 Shows the basic interface of the energy spectrum analysis. The user needs to provide the tube voltage, anode angle, target material, and filter thickness. They then click on “calculate” to obtain the X-ray energy spectrum and corresponding parameters. The width of the energy bin can be set to 1 keV or 2 keV, and the calculation results can be exported to the MCNP's source card.

3.2. Construction and validation of a CT scanner model

3.2.1. Construction of a CT scanner model

The experimental data used in this study were taken from a recent paper published in 2018 by Hassan et al. related to determination and verification of the bowtie of a CT scanner [12]. The measured CT scanner was a SOMATOM Definition 64 CT (Siemens Medical Solutions, Forchheim, Germany) and geometric parameters were listed in Table 3. The scanner has two bowties for small fields of view (SFOV) and large fields of view (LFOV). The material of the bowtie was presumed to be Teflon. According to physical measurements, the measured HVL was about 9.4 mm when the tube voltage was 140 kV. The equivalent X-ray energy spectrum was obtained by matching the measured with the calculated HVL values. Two bowtie filter thickness curves were obtained using the

Table 2
Comparison of results of CTMD with other energy spectrum softwares. All simulation results from MCNP5 had passed the mean behavior test, and all random relative uncertainties do not exceed 1%.

Tube voltage (kV)		BEAMnrc	SpekCalc	IPEM78	CTMD	Percentage Difference (%)
50	HVL (mm)	1.77	1.74	1.83	1.85	1.1–6.3
	E_{mean} (keV)	32.3	32.4	32.5	32.4	0.1–0.3
	E_{eff} (keV)	27.3	27.1	27.6	27.8	0.7–2.5
70	HVL (mm)	2.45	2.38	2.59	2.59	0.1–8.8
	E_{mean} (keV)	39.7	39.6	40.1	39.9	0.5–3.4
	E_{eff} (keV)	30.9	30.6	31.6	31.6	0.1–3.3
100	HVL (mm)	4.81	4.78	4.91	4.89	0.4–1.8
	E_{mean} (keV)	52.7	53.0	52.9	52.3	0.8–1.3
	E_{eff} (keV)	41.2	41.1	41.6	41.6	0.1–1.2
140	HVL (mm)	6.48	6.46	6.70	6.55	1.1–2.2
	E_{mean} (keV)	62.5	62.8	62.9	62.5	0.1–0.5
	E_{eff} (keV)	48.0	47.9	48.9	48.2	0.4–1.4

*The data for comparison was from Poludniowski's study.

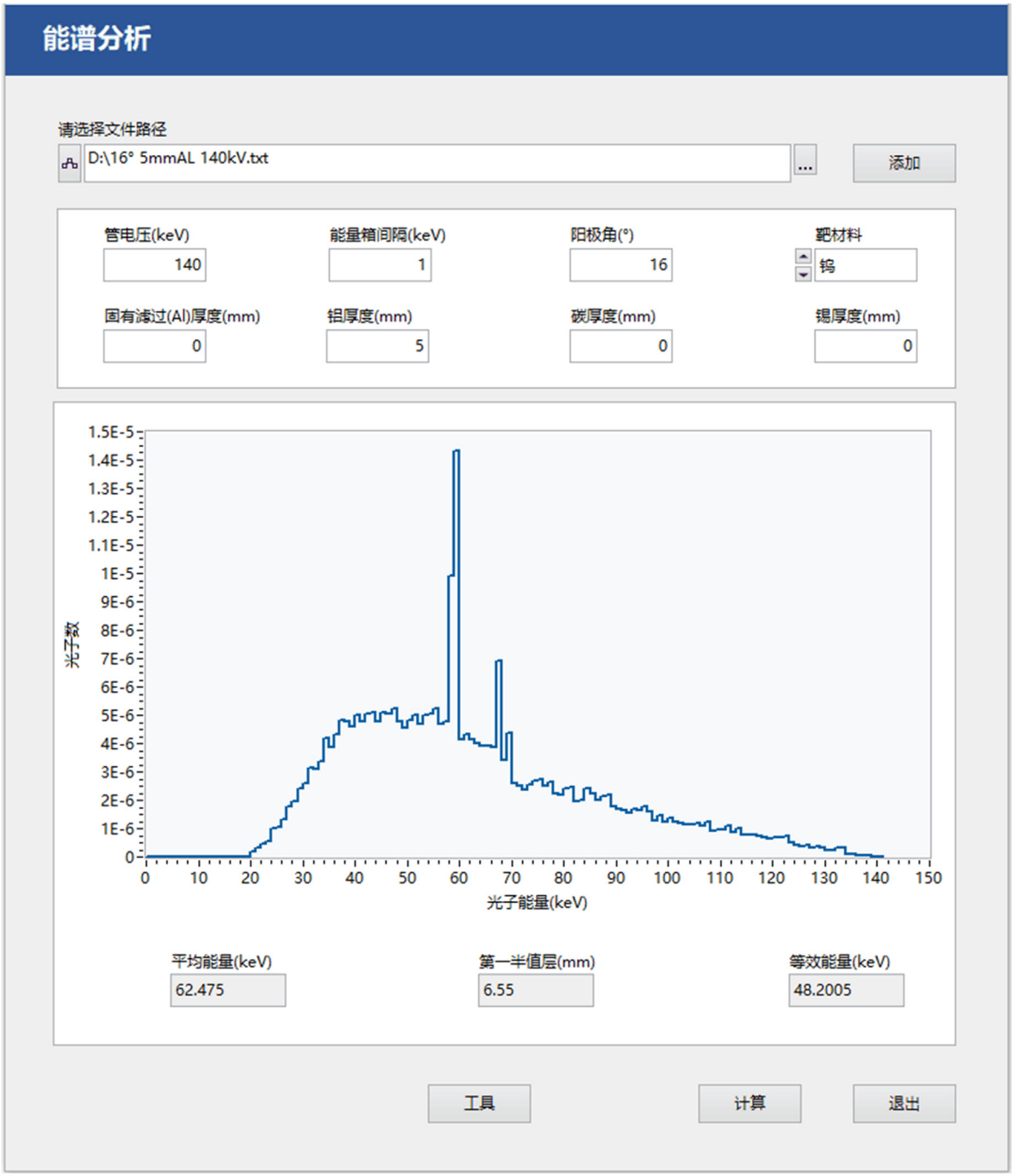

Fig. 3. Screenshot of energy spectrum analysis interface.

Table 3
Geometric and scanning parameters used in this study for constructing the CT scanner model.

Geometric parameters	Aperture of the gantry (cm)	78
	SID (mm)	59.5
	SDD (mm)	108.5
scanning parameters	Beam angle (°)	54
	Tube voltage (kV)	140
	Collimation (mm)	3.6
	HVL (mmAl)	9.4

SID = distance from the focal spot to the isocenter; SDD = distance from the focal spot to the detector; HVL = half-value layer.

physical measurements and calculations and the results were shown in Fig 4a and b, respectively.

The BT filter thickness as a function of fan angle was converted into a curve located in the Cartesian coordinate system. It can be seen from the results that it is difficult to use one quadratic curve to describe the bowtie filter shape because there is a turning point in the shape of the curve. In order to make the MC simulation results closer to the measurement results, Boolean operation with three quadratic curves and three rectangles was chosen as the construction method of the bowtie filter. The two constructed bowtie filter models shown in Labview's 3D window were shown in Fig 4c and d, respectively.

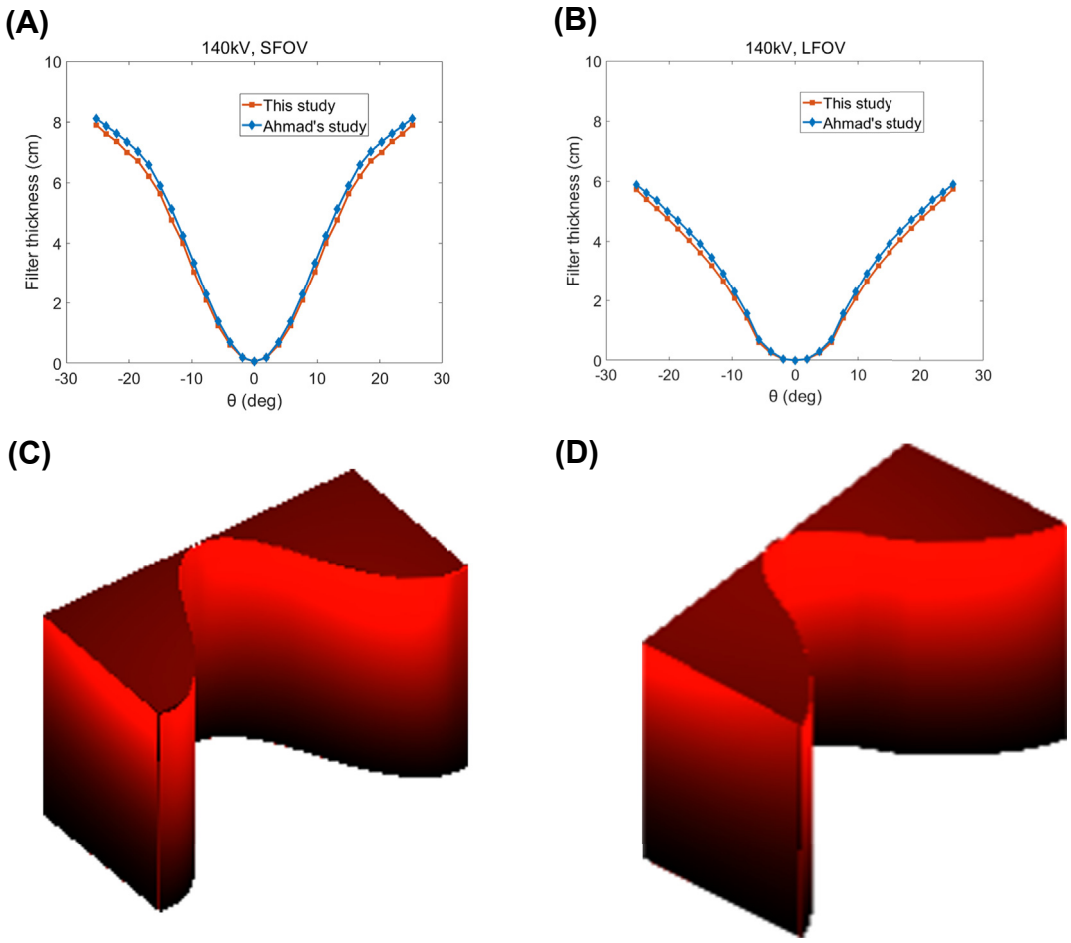

Fig. 4. The calculation results of the two types of BT filter shapes based on experimental data.

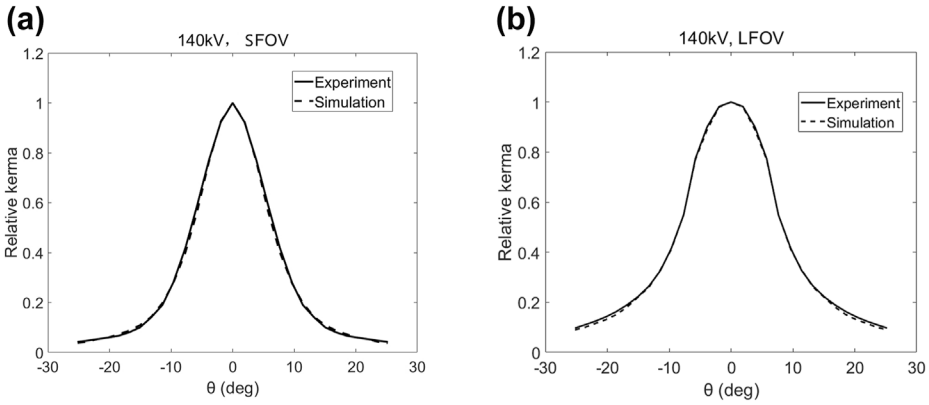

Fig. 5. Comparison of simulation and measurement results of the two types of BT filter shapes.

3.2.2. Comparison and validation of the CT scanner model

Based on the physical measurements and calculations, Hassan obtained normalized curves of air kerma as a function of fan angle at different tube voltages. The calculation results of filter thickness in this study were compared with those of Hassan's study, and the MC simulation results of this study were compared with experimental results.

As shown in Fig 4a and b, when the emission angle is within 10°, the calculation results of the bowtie filter thickness are very close to Hassan's study, and when the emission angle is greater than 10°, the calculation results of this study have an difference about 3% with Hassan's study. In general, for the equivalent spectrum obtained by matching the equal HVL value, the calculation results of bowtie thickness in this study are lower than Hassan's study.

Root mean square error (RSME) was used as the indicator to verify the accuracy of the CT scanner model constructed in this study, as in Hassan's study. For fairness, the settings of the ionization chamber parameters, measurement points and scanning conditions used for MC simulation in this study were the same as those in Hassan's study, and the energy conversion card was used to

converted the photon fluence to the air kerma. The simulation results correspond to two types of BT filters (SFOV and LFOV) and are shown in Fig. 5a and b, respectively. Compared to the measured normalization curve of air kerma, the RSME was 0.97% for SFOV and 0.74% for LFOV. In Hassan's study, the RSME was 1.16% for SFOV and 2.50% for LFOV under the same conditions. This proves that the CT scanner model obtained using the system developed in this study has achieved more accurate results, and the accuracy improvement effect for LFOV is more obvious.

3.3. Generation of the CT scanner system with the phantom

Fig. 6a shows the voxel matrix of the boundary representation (BREP) model of Chinese women of childbearing age established in our previous study. The voxel resolution of this model was 1.8 × 1.8 × 4.8 mm, which was constructed from the original CT pictures [26]. The final CT scanner system to describe the rotation process of the X-ray tube is shown in Fig. 6b. The scan length can be increased by changing the position of the source relative to the phantom. The organ doses can be calculated with energy deposition cards.

4. Discussion

It was found that there are some differences in the calculation results between different energy spectrum software, especially for the HVL, which was used to determine the equivalent X-ray energy spectrum. That causes the choice of the energy spectrum software

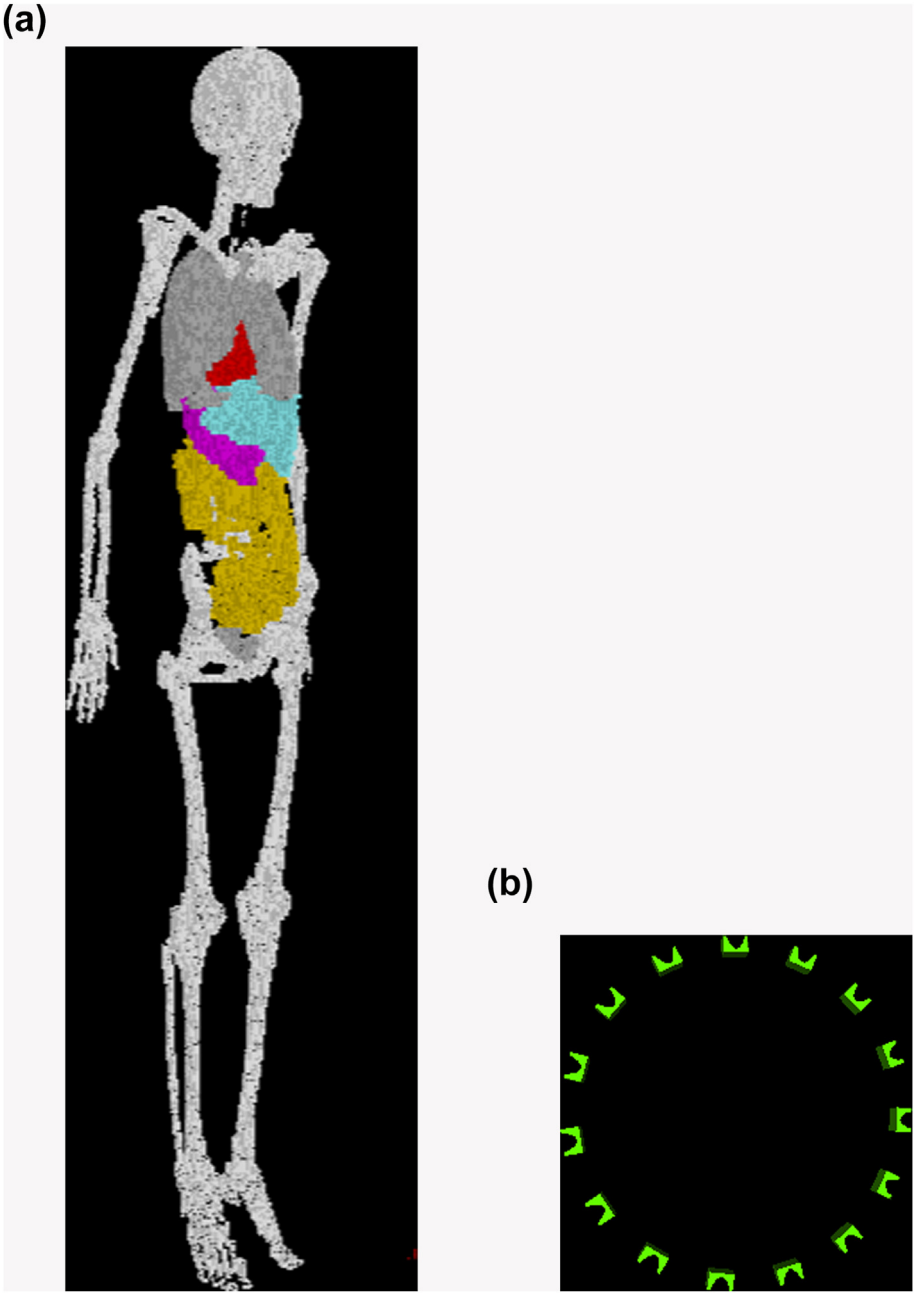

Fig. 6. (a) Screenshot of the voxel phantom (with part of the organs) preview window. (b) The final CT scanner model including the equivalent X-ray energy spectrum as well as the calculated BT shape and the phantom.

will affect the accuracy of the source model. However, this situation is rarely discussed in previous studies on CT scanner model construction. The difference between these calculation results may come from the difference of the energy spectrum model or the error in the fitting process of the energy attenuation and absorption curve. Some are calculated based on a semi-empirical model, some are simulated based on the MC algorithm, and some are a combination of the above two methods. The electronic transport algorithm will also affects the accuracy of the results. In MCNP5, the condensed history method, which includes the “ITS style” electron energy indexing and new detailed Landau energy straggling logic, is used to reduce the computation time of electron interactions at the cost of reducing the accuracy of the results [21]. It was verified that the simulation results from MCNP5 will bring more error for electron beams with energies lower than 0.1 MeV [27]. All of the above factors can lead todifferent inherent filtration of the X-ray tube given by different energy spectrum software even if the HVL value is the same.

In Hassan's study, SpekCalc was used to obtain the equivalent energy spectrum. According to the measurement results, when the tube voltage was 140 kV, the HVL was 9.4 mm (The measurement error was less than 1%) [12]. The calculated inherent filtration of the tube in Hassan's study was about 12mmAl. However, the calculated inherent filtration of the tube in this study was about 13mmAl, which was 8.3% different from the Hassan's study. According to the comparison results of the bowtie filter thickness calculation, as the attenuation of the X-ray energy increases, the difference in the calculation results of the bowtie thickness for different equivalent energy spectrum also increases, and this difference is not negligible. This indicates that the bowtie filter thickness calculated using different energy spectrum software will also be different, which leads to the difference of the constructed CT scanner model. At the same time, this explains from the side that the equivalent spectrum obtained by inputting the geometric parameters of the X-ray tube given by the manufacturer into a certain energy spectrum software cannot accurately describe the CT source model, and it will also bring errors to the calculation results of the radiation dose.

There are certainly differences in the CT source model due to the choice of the energy spectrum software, but more problems lie in that the database constructed by traditional energy spectrum software cannot meet the characteristics of some new types of X-ray tubes. For example, this software does not consider the alloy target, and have some limitations in terms of tube voltage. The advantage of the MC simulation method used in this study is that the user only needs to modify the input file according to the actual situation to get more accurate results. At the same time, the accuracy of MC simulation can also be guaranteed. The tube voltage is usually set to be above 80 kV when performing CT scanning. Under the same conditions, the higher the energy of the incident particle, the easier it is to interact with the matter [25]. Therefore, with higher tube voltage, the MC simulation error will decrease. This can explain why in the comparison results of different energy spectrum software, the calculated HVL values of this study at high tube voltage are closer to BEAMnrc, which is also developed based on MC simulation and calculation.

In the comparison and validation part of the CT scanner model, the simulation results of this study were very close to the measurement results provided by Hassan's study. The RSME for SFOV was 0.97%, and the RSME for LFOV was 0.74%, which were closer to experimental measurements than Hassan's simulation results. The reasons are divided into the following two aspects. First, when the tube voltage is 140 kV, the MC simulation results are more reliable, so for the same HVL value, the equivalent energy spectrum calculated in this study will be more accurate, which will promote the bowtie thickness calculation to be more accurate. Second, Hassan et al. used polynomial curves to describe the calculated bowtie shape, which will cause errors when constructing 3D geometric model. The same modeling idea was also used in Gu's study which proposed to use a cuboid minus an elliptical cylinder to simply describe the shape of the BT filter [5]. It is unknown whether the bowtie filters of different CT scanner models are different in general shape, but what is certain is that this model simplification method is not suitable for the description of all bowtie models. Therefore, a more reliable method is to accurately build a 3D model of the bowtie shape based on measurement data. The system developed in this study takes advantage of Labview's geometric calculations, and can obtain a more accurate 3D model of the bowtie shape by splicing three quadric surfaces with a rectangular parallelepiped. The improvement of the accuracy of the CT model by this modeling method is well reflected in the bowtie filter for LFOV, because the turning point of this bowtie shape curve was more obvious.

There is also a parameter that is easy to be ignored when constructing a CT scanner model, that is, SFD. SFD can hardly be provided by the manufacturer, but its value directly affects the shape of the bowtie. For the same energy attenuation, the larger the SFD value, the thinner and wider the bowtie filter. Although this change cannot affect the accuracy of the simulation results, it affects the CT scanner system model, because 16 sources are needed to simulate one rotation of the X-ray tube. If the bowtie model is too wide, the model will overlap and calculation will report an error. Therefore, when constructing the bowtie filter model, an appropriate SFD value should be selected.

In all, in order to obtain an accurate CT scanner model, it is necessary to avoid relying on the manufacturer's parameters and take the physical measurements as the standard. First, by matching the HVL value under different tube voltages to obtain the equivalent energy spectrum. The matched energy spectrum library needs to be established based on MC simulation, and the input file can be modified to suit the actual situation of the tube. Then, the bowtie shape curve is obtained by using the equivalent energy spectrum and the static X-ray source measurements. Pay attention to the turning point of the curve shape. It is necessary to use the three-segment splicing modeling method to construct the bowtie filter model. Finally, verify the constructed CT scanner model through MC simulation.

5. Conclusions

This study has innovatively solved several key issues of CT sacnner model construction in MC simulations by an user-friendly system developed on LabVIEW. It has solved the limitations of MCNP's drawing function through 3D display function and also helps researchers to write MCNP input files. After comparison with an example, it was proved that the calculation and modeling method of this study can obtain a more accurate CT model, and therefore can obtain a more accurate radiation dose. In the final discussion part, this study has analyzed and proposed methods to improve the CT scanner model from both physical principles and model construction methods, which is meaningful for calculating the patient dose obtained from a CT scanner.

Further studies will add new calculation methods to this system. CTMD currently only supports calculations of single-energy X-ray tubes and single layer BT filters. These are only suitable for single-energy CT scanner model construction. For example, new dual-energy CTs such as the Siemens 64-detector-row dual-energy CT Definition Flash have two layers of BT filters with structures based on different materials. More experimental measurements are required to construct such an advanced CT sacnner model.

Declaration of competing interest

The authors declare that they have no known competing financial interests or personal relationships that could have appeared to influence the work reported in this paper.

Acknowledgements

This work was supported by the National Natural Science Foundation of China (No. 82073474) and the Planning Project of Shanghai Science and Technology (No. 21S31902100). We would like to thank Weihai Zhuo and Haikuan Liu (Institute of Radiation Medicine, Fudan University, Shanghai, China) for their suggestions with regard to writing.

References

[1] F.B. Brown, MCNP—A General Monte Carlo N-Particle Transport Code, Version 5, LA-UR-03-1987, Los Alamos, Los Alamos National Laboratory, 2003.
[2] X Monte Carlo Team, MCNP - A General Monte Carlo N-Particle Transport Code, Version 5,Volume II: User's Guide, Los Alamos National Laboratory, Los Alamos, NM, 2003.
[3] G. Jarry, J.J. DeMarco, U. Beifuss, C.H. Cagnon, M.F. McNittGray, A Monte Carlo-based method to estimate radiation dose from spiral CT: from phantom testing to patient-specific models, Phys. Med. Biol. 48 (2003) 2645–2663.
[4] A.C. Turner, D. Zhang, H.J. Kim, J.J. DeMarco, C.H. Cagnon, E. Angel, D.D. Cody, D.M. Stevens, A.N. Primak, C.H. McCollough, M.F. McNitt-Gray, A method to generate equivalent energy spectra and filtration models based on measurement for multidetector CT Monte Carlo dosimetry simulations, Med. Phys. 36 (2009) 2154–2164.
[5] J.W. Gu, B. Bednarz, X.G. Xu, S.B. Jiang, Assessment of patient organ doses and effective doses using the VIP-Man adult male phantom for selected conebeam CT imaging procedures during image guided radiation therapy, Radiat. Protect. Dosim. 131 (2008) 431–443.
[6] C. Lee, K.P. Kim, D. Long, R. Fisher, C. Tien, S.L. Simon, A. Bouville, W.E. Bolch, Organ doses for reference adult male and female undergoing computed tomography estimated by Monte Carlo simulations, Med. Phys. 38 (2011) 1196–1206.
[7] S.E. McKenney, A. Nosratieh, D. Gelskey, K. Yang, S.Y. Huang, L. Chen, J.M. Boone, Experimental validation of a method characterizing bowtie filters in CT scanners using a real-time dose probe, Med. Phys. 38 (2011) 1406–1415.
[8] K. McMillan, M. McNitt-Gray, D. Ruan, Development and validation of a measurement-based source model for kilovoltage cone-beam CT Monte Carlo dosimetry simulations, Med. Phys. 40 (2013), 111907.
[9] A.P. Colijn, W. Zbijewski, A. Sasov, F.J. Beekman, Experimental validation of a rapid Monte Carlo based micro-CT simulator, Phys. Med. Biol. 49 (2004) 4321–4333.
[10] M. Randazzo, M. Tambasco, A rapid noninvasive characterization of CT x-ray sources, Med. Phys. 42 (2015) 3960–3968.
[11] J.M. Boone, Method for evaluating bowtie filter angle-dependent attenuation in CT: theory and simulation results, Med. Phys. 37 (2010) 40–48.
[12] A.I. Hassan, M. Skalej, H. Schlattl, C. Hoeschen, Determination and verification of the x-ray spectrum of a CT scanner, J. Med. Imaging 5 (2018), 013506.
[13] K. Cranley, B.J. Gilmore, G.W.A. Fogarty, L. Deponds, Catalogue of Diagnostic X-Ray Spectra and Other Data IPEM, IPEM, York, 1997. Report No. 78.
[14] R. Birch, M. Marshall, Computation of bremsstrahlung x-ray spectra and comparison with spectra measured with a Ge(Li) detector, Phys. Med. Biol. 24 (1979) 505–517.
[15] D.W.O. Rogers, C.M. Ma, G.X. Ding, B. Walters, D. Sheikh-Bagheri, G.G. Zhang, NRCC Report PIRS-0509(A)revK: BEAMnrc Users Manual, NRCC, Ottawa, 2004.
[16] G. Poludniowski, G. Landry, F. DeBlois, P.M. Evans, F. Verhaegen, SpekCalc: a program to calculate photon spectra from tungsten anode x-ray tubes, Phys. Med. Biol. 54 (2009) 433–438.
[17] N. Zaker, M. Zehtabian, S. Sina, C. Koontz, A.S. Meigooni, Comparison of TG-43 dosimetric parameters of brachytherapy sources obtained by three different versions of MCNP codes, J. Appl. Clin. Med. Phys. 17 (2016) 379–390.
[18] D. Barbesi, V.V. Vicente, S. Millet, M. Sandow, J.Y. Colle, D.L.H.L. Aldave, A LabVIEW®-based software for the control of the AUTORAD platform: a fully automated multisequential flow injection analysis Lab-on-Valve (MSFIA-LOV) system for radiochemical analysis, J. Radioanal. Nucl. Chem. 313 (2017) 217–227.
[19] G.G. Poludniowski, P.M. Evans, Calculation of x-ray spectra emerging from an x-ray tube. Part I. electron penetration characteristics in x-ray targets, Med. Phys. 34 (2007) 2164–2174.
[20] Y. Kong, W. Zhuo, B. Chen, C. Zhao, MCNP simulations of medical diagnostic X-ray spectra, Nuclear Technioues 42 (2019) 11.
[21] X-5 Monte Carlo Team, MCNP—A General Monte Carlo N-Particle Transport Code, Version 5 Volume I: MCNP Overview and Theory, Los Alamos National Laboratory, NM, 2003. Report No. LA-UR-03-1987.
[22] M.G. David, E.J. Pires, M.A. Bernal, J.G. Peixoto, C.E. Dealmeida, Experimental and Monte Carlo-simulated spectra of standard mammography-quality beams, Br. J. Radiol. 85 (2012) 629–635.
[23] S.M. Seltzer, Calculation of photon mass energy-transfer and mass energy-absorption coefficients, Radiat. Res. 136 (1993) 147–170.
[24] J. Gu, B. Bednarz, P.F. Caracappa, X.G. Xu, The development, validation and application of a multi-detector CT (MDCT) scanner model for assessing organ doses to the pregnant patient and the fetus using Monte Carlo simulations, Phys. Med. Biol. 54 (2009) 2699–2717.
[25] M. Cros, R.M.S. Joemai, J. Geleijns, D. Molina, M. Salvadó, SimDoseCT: dose reporting software based on Monte Carlo simulation for a 320 detector-row cone-beam CT scanner and ICRP computational adult phantoms, Phys. Med. Biol. 62 (2017) 6304–6321.
[26] H. Zhang, S. Sun, H. Lu, Y. Liu, Construction and application of BREP phantom for Chinese women of childbearing age in radiation protection, Radiat. Protect. Dosim. 189 (2020) 407–419.
[27] H. Koivunoro, T. Siiskonen, P. Kotiluoto, I. Auterinen, E. Hippelainen, S. Savolainen, Accuracy of the electron transport in mcnp5 and its suitability for ionization chamber response simulations: a comparison with the egsnrc and penelope codes, Med. Phys. 39 (2012) 1335–1344.